Article

Initial Approach to Self-Compacting Concrete with Raw-Crushed Wind-Turbine Blade: Fresh, CFD and Mechanical Analysis

Manuel Hernando-Revenga [1], **Víctor Revilla-Cuesta** [1], **José A. Chica** [2], **Vanesa Ortega-López** [1,*] **and Juan M. Manso** [1]

[1] Department of Civil Engineering, University of Burgos, 09001 Burgos, Spain; mhrevenga@ubu.es (M.H.-R.); vrevilla@ubu.es (V.R.-C.); jmmanso@ubu.es (J.M.M.)

[2] TECNALIA, Basque Research and Technology Alliance (BRTA), 48160 Bizkaia, Spain; joseantonio.chica@tecnalia.com

[*] Correspondence: vortega@ubu.es; Tel.: +34-947-259073

Abstract: The production of raw-crushed wind-turbine blade (RCWTB) and its addition to conventionally designed self-compacting Concrete (SCC) enable us to provide a second life to wind-turbine blades. However, SCC containing RCWTB must show proper fresh behavior, an aspect evaluated in this paper both experimentally and through simulations based on computational fluid dynamics (CFD) for RCWTB additions up to 3.0% by volume. In experimental terms, RCWTB reduced the flowability and passing ability of SCC, and slowed SCC flow, although the performance of SCC with 1.5% RCWTB was adequate under free-flow conditions. In terms of modeling, RCWTB did not impact yield stress and increased plastic viscosity. CFD modeling under free flow, regardless of the presence or not of obstacles simulating concrete reinforcement, was successful, especially in the long term. Nevertheless, the modeling of the passing ability was not accurate; precision could be improved by simulating the effect of the individual GFRP fibers within the SCC flow. Finally, the mechanical properties of SCC were negatively impacted by RCWTB, the stitching effect of the GFRP fibers not being effective in an SCC with a conventional design. A specific SCC design when adding RCWTB is therefore needed to advance in the use of this waste in this concrete type.

Keywords: raw-crushed wind-turbine blade; self-compacting concrete; flowability; passing ability; computational fluid dynamics; Bingham equation

1. Introduction

Self-compacting concrete (SCC) is a type of concrete with high-performance fresh behavior [1]. Its high flowability and low viscosity allows free flowing and proper formwork filling without compaction, which in turn saves energy [2]. This optimal fresh behavior makes it the preferred type of concrete when there are large pumping heights [3], when the reinforcement of a structural element is very heavy [4], and in the precast-concrete industry, since the reduction of energy consumption due to vibration allows for cost savings [5]. This high flowability is achieved with a specific composition, which is based on a high proportion of fine aggregate (size less than 0.063 mm) [6], an adjusted content of coarse aggregate [7], and the use of superplasticizers [8].

SCC composition has major importance, since any modification to it alters SCC fresh behavior [6,7], which may even cause the concrete mix to lose its self-compactability [9]. Thus, the impact of any alternative raw material must be examined in great detail:

- First, the so-called alternative or sustainable aggregates can be mentioned. Their usually irregular shape causes them to exhibit greater friction with other SCC components when dragged by the cement paste [4,10]. The cement paste of SCC therefore needs to be denser and more compact in order to be able to achieve proper flowability [11]. They also affect the granular skeleton and, in turn, the packing level when fresh [12,13].

Furthermore, each of them has its own peculiarity. For example, recycled concrete aggregate shows high water-absorption levels [14], which, if not compensated for in the mix design, will make SCC insufficiently flowable [15]. Another example is electric arc furnace slag, an aggregate with a high density [16] that requires SCC to have a cement paste with a high proportion of aggregate particles of less than 0.50 mm to reach a sufficient high dragging capacity [17].

- Second, there are alternative binders. They enable the cement content of SCC to be reduced, thus improving its sustainability [18,19]. However, they have different characteristics than ordinary Portland cement, which alter the cement-paste dragging capacity [18]. Some of the most studied examples are ground granulated blast-furnace slag and silica fume. Ground granulated blast-furnace slag has a higher ground fineness than conventional cement (higher specific surface area) [20], which decreases the compactness of the cement paste [21]. This in turn means that a SCC with good performance in the fresh state can only be achieved if the coarse-aggregate content is adjusted, commonly reducing it [22]. Silica fume tends to agglomerate [23], hindering the creation of a workable cement paste [24]. In this case, a proper mixing process that ensures its adequate dispersion is key to achieve self-compactability [25].

- Fibers are the last concrete component to be highlighted. These elements act as a three-dimensional reinforcement in hardened concrete, which increases flexural strength, reduces shrinkage and improves durability by limiting the formation and propagation of cracks [26,27]. However, their impact on the fresh state of the SCC is negative, as they interfere with the movement of the rest of the SCC components, mainly hindering the flow of the coarse aggregate [28]. A sufficiently compact cement paste in the fresh state by a proper amount of fine aggregate and adding an adequate proportion of fibers is key for SCC manufacturing when adding fibers [9,28].

The blades from dismantled wind turbines currently cause a great environmental impact, as the recycling of their constituent materials is not easy [29,30]. These constituents are basically glass fiber-reinforced polymer (GFRP), balsa wood, and different types of polymers, which are usually glued together [31]. Furthermore, the need to find a solution for the recycling of such wind-turbine components is becoming increasingly pressing. In Europe alone, it is estimated that 77,000 wind-turbine blades will need to be recycled over the next 20 years [32]. One of the recycling possibilities has been the separation of these constituents by cutting and then managing them separately [33,34]. Polymers and balsa wood can be easily managed in this way, but GFRP recycling still remains complicated [35]. One possible route whose validity has been researched is a thermal and chemical process to separate the glass fibers from the polymer matrix [36], but the mechanical properties of fiberglass are significantly degraded, which hinders their use [37]. Another research avenue has been the mechanical crushing of GFRP, which yields GFRP fibers that can be used as a concrete component and eliminates the need to separate the GFRP constituents [33,38]. These GFRP fibers provide load-bearing capacity to concrete [39].

The authors of this research are currently going a step further and are evaluating the suitability of the simultaneous crushing of all the constituents of wind-turbine blades. This mechanical treatment leads to raw-crushed wind-turbine blade (RCWTB) [40], and simplifies the recycling process, as all the constituents of the wind-turbine blades can be managed simultaneously [33,36]. This waste is composed not only of GFRP fibers, but also of polymer and balsa-wood particles, with an approximately spherical shape [40]. Its use in contents of up to 6% by volume for the production of concrete of conventional workability has been successful, even improving its flexural strength [41]. Thus, the next step in this line of research is to propose the use of this waste for the manufacture of SCC. However, a preliminary evaluation of how the reduced RCWTB content affects the flowability of SCC is needed in order to later advance the formulation of a suitable SCC when adding this waste [17,42]. This aspect, which has yet to be covered in the concrete-science literature to date, is evaluated in this scientific paper.

The evaluation of SCC flowability through laboratory tests is the most common way to know the impact of the use of an alternative raw material on fresh SCC. Nevertheless, this experimental evaluation requires time and specific equipment [43]. Fluid simulation tools such as computational fluid dynamics (CFD) can soften that analysis, apart from allowing it to deepen the flowability of SCC in terms of viscosity [44]. CFD can model any fluid as homogeneous and divide it into uniform small elements to which mathematical equations describing the fluid motion are applied [45]. The solution of those equations simulates fluid movement and flow patterns [2]. When applied to SCC, CFD can focus on flowability, pumping processes, and fiber movement within the cement paste [46]. Nevertheless, the non-Newtonian behavior of SCC has to be considered for a successful simulation [47]. Although different constitutive laws can be used for that, the Bingham equation is usually chosen due to its simplicity and faithful similarity to real behavior [48].

The fresh performance of SCC containing up to 3% by volume of RCWTB is analyzed both experimentally and through CFD in this research. Simulations are conducted based on experimental measurements of the free flow of SCC to elucidate the effect of RCWTB on the viscosity of SCC and to define its relationship with the free-flow experimental results. From that point, the passing ability of SCC is also modeled through CFD with the aim of evaluating the suitability of this methodology to explain it. Finally, the mechanical properties of the SCC mixes are briefly addressed to offer an overview of SCC behavior. The goal is initially approaching the behavior of conventionally designed SCC with RCWTB to provide a new path for the re-evaluation of wind-turbine blades.

2. Materials and Methods

2.1. Raw Materials

2.1.1. Conventional Raw Materials

SCC was composed of CEM II/A-L 42.5 R cement, superplasticizers, water, siliceous gravel 4/12 mm, siliceous sand 0/4 mm, and limestone sand 0/2 mm.

- Cement was standardized as per EN 197-1 [49]. Its main characteristic was a limestone content between 6% and 20% by weight, which allowed reducing the environmental impact related to cement use [19].
- The superplasticizers were polycarboxylate-based. They had been used in previous research by the authors, in which they showed adequate performance when used to produce SCC [5,22]. The water was provided by the municipal water supply.
- Three aggregate fractions were considered to reach adequate aggregate-particle packing, thus providing the SCC with a suitable granular skeleton [17]. Furthermore, limestone sand 0/2 mm provided the necessary fine aggregate content to achieve SCC [50]. The appearance of the aggregates is shown in Figure 1. Their chemical and physical properties are detailed in Table 1, and their gradations are depicted in Figure 2.
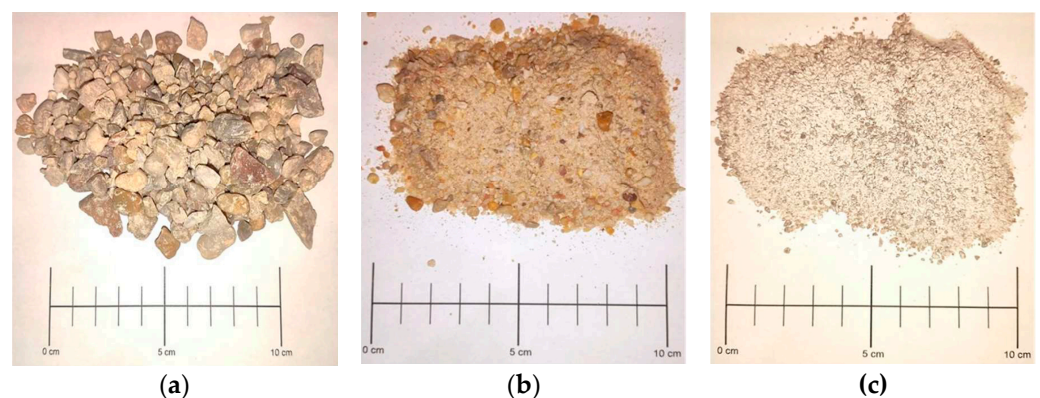

**Figure 1.** Aggregates used in SCC production: (**a**) siliceous 4/12 mm; (**b**) siliceous 0/4 mm; (**c**) limestone 0/2 mm.

Table 1. Physical and chemical properties of aggregates.

Property	Standard	Siliceous 4/12 mm	Siliceous 0/4 mm	Limestone 0/2 mm
Fine content (%)	EN 933-1 [51]	0.3	1.5	2.0
Equivalent sand (%)	EN 933-8 [52]	-	77	79
Saturated-surface-dry density (Mg/m^3)	EN 1097-6 [53]	2.66	2.65	2.64
Water absorption (% wt.)	EN 1097-6	0.66	0.74	0.52
Flakiness index (% wt.)	EN 933-3 [54]	4.5	-	-
Water soluble chloride content (% wt.)	EN 1744-1 [55]	0.00	0.00	0.01
Sulfur content (% wt.)	EN 1744-1	0.00	0.01	0.01
Acid soluble sulfates (% wt.)	EN 1744-1	0.01	0.01	0.02
Light pollutants (%wt.)	EN 1744-1	0.00	0.00	0.01
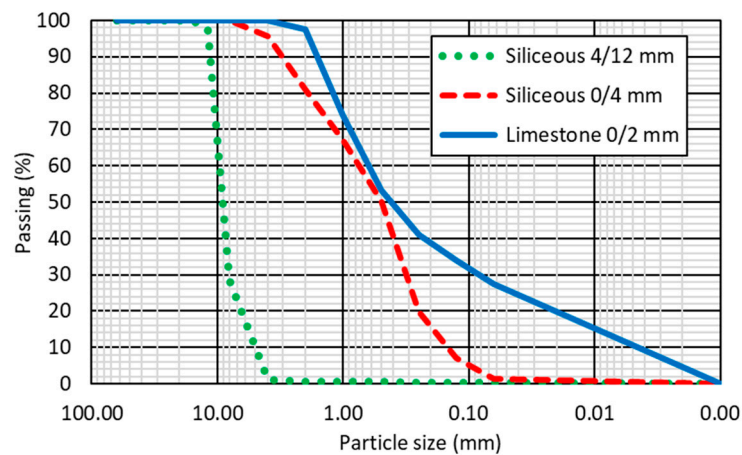
Figure 2. Aggregates' gradation.

2.1.2. Raw-Crushed Wind-Turbine Blade (RCWTB)

The RCWTB used for SCC development was obtained by shredding panels of wind-turbine blades such as those shown in Figure 3a. These panels were composed of GFRP, balsa wood, and polymers. They were first cut into roughly square pieces with a side length of around 20 cm, and then crushed by a knife mill and screened with a sieve with a mesh size of 10 mm. Those particles that did not pass through the sieve were crushed again until the particles passed. The resulting material can be seen in Figure 3b, which had a real density of 1.63 Mg/m^3 (EN 1097-6 [53]).

(**a**)

(**b**)
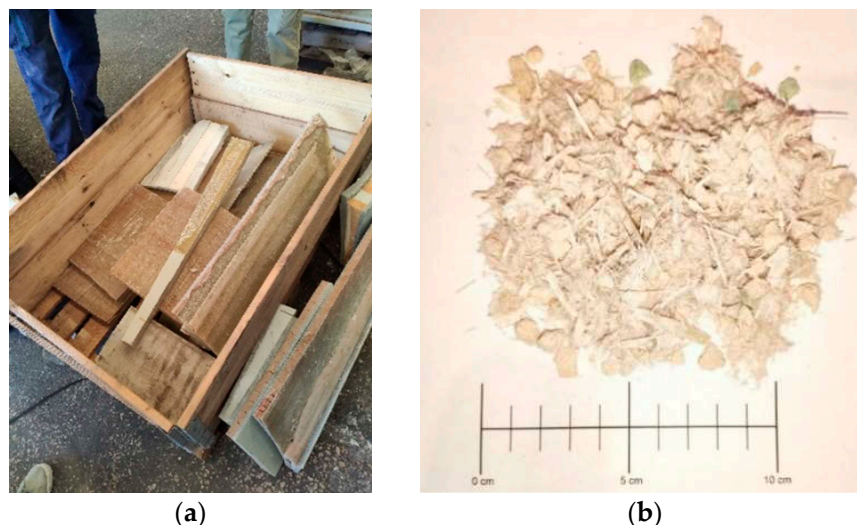
Figure 3. Panels of wind-turbine blades (**a**) and RCWTB (**b**).

The RCWTB was composed of balsa-wood particles (6.3% wt.), polymer particles (8.3% wt.), GFRP micro-fibers and small non-separable particles (18.6% wt.), which were agglomerated in the form of fluffs, and GFRP fibers (66.8% wt.). All these components can be seen in Figure 4. The particles of polymers and balsa wood could act as lightweight aggregates in the SCC [56], and the GFRP fibers could form a three-dimensional reinforcement in the hardened SCC, but also negatively affect its flowability in the fresh state [28]. The fibers exhibited a 13.1-mm average length, and an average tensile strength of 270 MPa. A much more detailed description of this material is shown in the previous work of the research group [40].
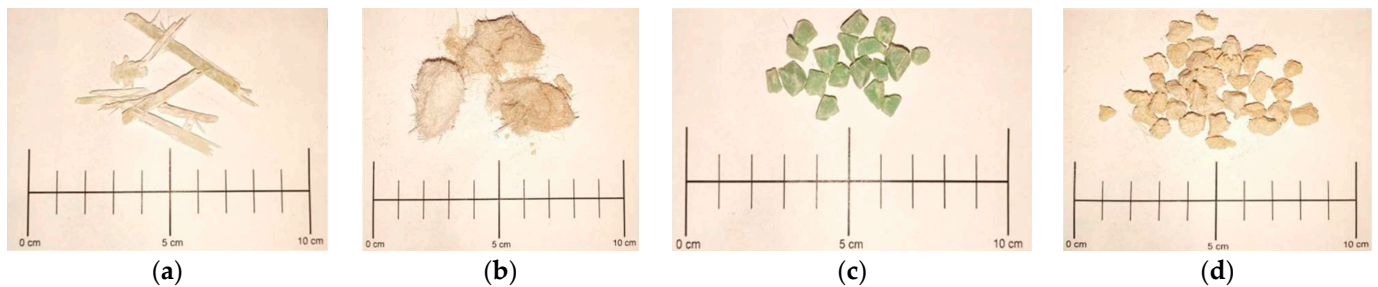

| (a) | (b) | (c) | (d) |

Figure 4. RCWTB components: (**a**) GFRP fibers; (**b**) GFRP micro-fibers and small non-separable particles; (**c**) polymers; (**d**) balsa wood.

2.2. SCC Design

Conventional SCC design following the previous experience of the authors in SCC with different wastes was conducted [9,17,22]. SCC with 0% vol. RCWTB (*RW* mix) was first designed to reach an SF2 slump-flow class as per EN 206 [57]. To perform this, 320 kg/m^3 of cement, a water/cement ratio of 0.48, and a superplasticizer amount of 2.4% wt. of cement mass were considered. Furthermore, the joint gradation of the aggregates was determined by Faury's curve, although the amount of fine aggregate was defined through the Fuller's aggregate gradation, as can be observed in Figure 5. In this way, both adequate particle packing and fine aggregate content were ensured [7].
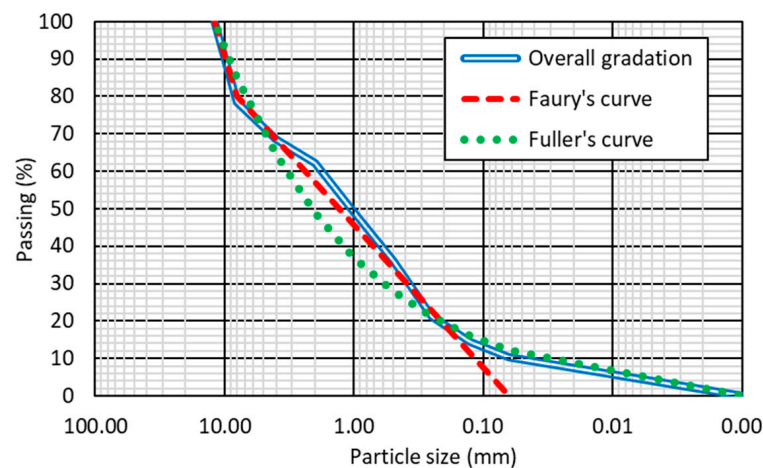
Figure 5. Overall gradation of the aggregates.

1.5% vol. and 3.0% vol. RCWTB (*W*1.5 and *W*3.0 mixes) were subsequently added to SCC as overall additions. The water/cement ratio was increased by around 0.08 per 1.5% RCWTB to partially compensate its negative effect on flowability according to our experience [40]. The superplasticizer content was not modified in order not to introduce more variables that could affect the fresh behavior of the SCC, since this research was the first approach for the development of SCC containing RCWTB.

The composition of the three SCC mixes developed in this study is detailed in Table 2. The use of RCWTB as an overall addition while maintaining the amount of the rest of the components constant caused the volume of SCC produced to increase, as can be perceived in the last row of Table 2. Thus, the composition of SCC is shown both in comparative terms and in kg/m^3 in it. The former allows us to comprehend the proportioning of the mixes comparatively, while the latter allows us to understand the decrease in cement content caused by the addition of RCWTB. Therefore, the use of RCWTB also increased the sustainability of SCC, similar to its use in conventional-workability concrete [41].

Table 2. SCC composition.

Component	Comparative Composition			kg/m^3 Composition		
	RW	*W1.5*	*W3.0*	*RW*	*W1.5*	*W3.0*
Cement	320	320	320	318.8	305.1	293.9
Water	155	185	210	154.4	176.4	192.9
Limestone sand 0/2 mm	680	680	380	677.4	648.3	624.5
Siliceous sand 0/4 mm	660	660	660	657.5	629.3	606.1
Siliceous gravel 4/12 mm	600	600	600	597.7	572.1	551.0
Superplasticizers	6.7	6.7	6.7	6.7	6.4	6.1
RCWTB	0.0	24.5	49.0	0.0	23.4	45.0
Volume (liters)	1004	1049	1089	1000	1000	1000

2.3. Experimental Tests in the Fresh State

Fresh tests were performed to evaluate the flowability and passing ability of SCC. Slump-flow, 3-bar L-box, and 16-bar J-ring tests were conducted according to EN 12350-8 [58], EN 12350-10 [59], and EN 12350-12 [60], respectively. Three determinations were performed for each test in each SCC mix.

- The slump-flow test (Figure 6a) consisted of allowing the free flow of SCC after putting it into the Abrams cone and carefully lifting it in a vertical direction. The maximum spreading diameter in two perpendicular directions was measured, whose average value is named SCC slump flow. The time that SCC took to reach a slump flow of 500 mm was also recorded (t_{500} time) [22].

(a) (b) (c)
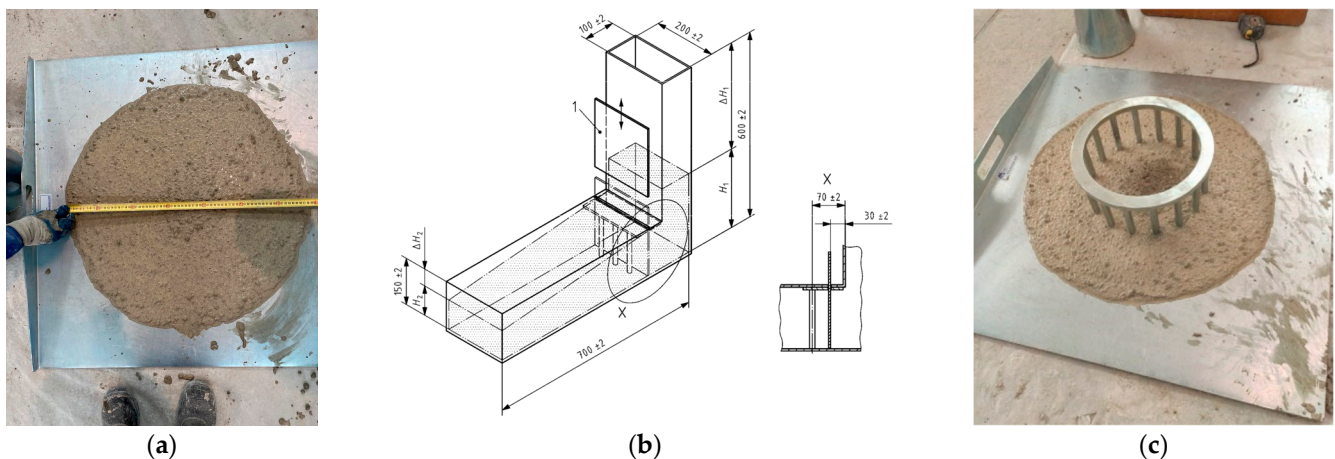
Figure 6. Fresh tests in SCC: (**a**) slump-flow test; (**b**) 3-bar L-box test ("1" is the gate; dimensions in mm) according to EN 12350-10 [59]; (**c**) 16-bar J-ring test.

- The 3-bar L-box test (Figure 6b) involved placing SCC in the vertical part of a 90-degree box. After that, a door located at the bottom of the vertical zone was opened, which allowed the concrete to flow through three bars simulating concrete reinforcement. The SCC flowed along the horizontal zone, with the SCC height being measured both

at the end of the horizontal zone and before the gate when the SCC flow ended. The quotient between these two heights is named blocking ratio, which is the result of this test [28].

- Finally, the 16-bar J-ring test (Figure 6c) was performed identically to the slump-flow test, but placing a ring in the center of the concrete flow zone whose bars simulated concrete reinforcement. The same values as in the slump-flow test were measured, along with the difference in the height of SCC between the ring's center and immediately after the bars to evaluate the passing capacity of SCC. This value is referred to as the J-ring blocking ratio.

Depending on the values obtained in each fresh-behavior test, SCC is assigned different classifications according to the indications of the European Federation of National Associations Representing for Concrete (EFNARC) [61], also detailed in the EN 206 standard [57]. These classifications provide a clear and quick approach to the fresh performance of SCC based on an experimental assessment. The classifications for the slump-flow, 3-bar L-box, and 16-bar J-ring tests are detailed in Table 3.

Table 3. SCC classes according to experimental fresh-state tests.

Test	Parameter	Class	Condition
		SF1	Slump flow between 550 mm and 650 mm
	Slump flow	SF2	Slump flow between 650 mm and 750 mm
Slump-flow test		SF3	Slump flow between 750 mm and 850 mm
	t_{500} time	VS1	t_{500} time lower than 2 s
		VS2	t_{500} time higher than 2 s
3-bar L-box test	Blocking ratio	PA2	Blocking ratio in a 3-bar L-box test higher than 0.80
		J-ring SF1	J-ring slump flow between 550 mm and 650 mm
	Slump flow	J-ring SF2	J-ring slump flow between 650 mm and 750 mm
16-bar J-ring test		J-ring SF3	J-ring slump flow between 750 mm and 850 mm
	t_{500} time	J-ring VS1	J-ring t_{500} time lower than 2 s
		J-ring VS2	J-ring t_{500} time higher than 2 s
	Blocking ratio	PJ2	Blocking ratio in a 16-bar J-ring test lower than 10 mm

2.4. CFD-Simulation Approach

Once the fresh behavior of SCC containing RCWTB was experimentally characterized, it was simulated using CFD tools through the results of the slump-flow test with the objective of deepening the effect of this residue on the viscosity of SCC. It was also sought to analyze the relationship of viscosity with the passing ability of SCC, measured through the blocking ratios of the 3-bar L-box and 16-bar J-ring tests. The Bingham equation was considered for such simulation, which is defined in Equation (1), in which τ is the shear stress in Pa; τ_0 denotes the yield stress in Pa; μ refers to the fluid's plastic viscosity in Pa·s; and $\dot{\gamma}$ means the shear rate in s^{-1}.

$$\begin{cases} \tau = \tau_0 + (\cdot\dot{\gamma}) & \tau > \tau_0 \\ \dot{\gamma} = 0 & \tau \leq \tau_0 \end{cases} \tag{1}$$

Flow3D® software (v2023R2 version), developed by Flow Science, was the CFD tool used for the CFD simulations [62]. On the one hand, this software is conceived to simulate free-surface flows. On the other hand, the TruVOF algorithm with which it works allows us to model dynamic free surfaces in a very accurate way. Finally, its interface and post-processing module are simple and intuitive, facilitating data analysis. From all this, this software perfectly enabled us to address the flow conditions of SCC containing RCWTB.

The slump-flow test was first simulated. For this purpose, the Abrams cone and the SCC volume were geometrically modeled and imported into the Flow3D® software. Subsequently, boundary conditions were defined, which consisted of imposing a flow under the gravity action and establishing the initial motion of lifting the Abrams cone,

as it defined the beginning of the flow of SCC. Finally, a mesh size of 1/3 mm was established, since such size enabled us to balance the accuracy of the simulation and the computational time [63]. Iterative simulations were conducted by fixing values for the parameters τ_0 and μ of the Bingham equation and considering time steps of 0.5 s until the end of the test, in order not to excessively increase the computational time. Different values of Bingham's parameters were considered until the simulation results matched the experimental ones with a difference lower than 5% on average, in line with previous studies [64]. The viscosity law (Equation (2); η_{av}, apparent viscosity in Pa·s) could also be defined from the Bingham equation.

$$\eta_{av} = \mu + \left(\frac{\tau_0}{\dot{\gamma}} \right) \tag{2}$$

L-box and J-ring tests were then simulated using CFD. Following the geometrical modelling of both the equipment of the tests and the SCC volume, the boundary conditions were fixed. These conditions were the flow under the gravity action and the motion of opening the L-box gate (3-bar L-box test) or lifting the Abrams cone (16-bar J-ring test). A mesh size of 1/3 mm and time steps of 0.5 s were also considered, as in the slump-flow test. The goal was to obtain the error rates of these tests compared to the experimental results with the aim of assessing the validity of CFD to analyze the passing ability of SCC with RCWTB.

2.5. Mechanical Properties

To conclude this first approach to the development of SCC with RCWTB, the mechanical properties of the three mixtures were evaluated. Fifteen cylindrical specimens with a height of 20 cm and a diameter of 10 cm, and three prismatic specimens with a height and width of 7.5 cm and a length of 27.5 cm were prepared. These specimens were stored in a humid chamber at a temperature of 20 ± 2 °C and a relative humidity of $90 \pm 5\%$ until the age of testing following the EN 12390-2 standard [65]. The tests performed, along with the standards, the testing age, and the specimens used were as follows:

- Compressive strength (EN 12390-3 [66]) at 7, 28 and 90 days in three cylindrical specimens per age.
- Elastic modulus (EN 12390-13 [67]) at 28 and 90 days in three cylindrical specimens. The same specimens were used at both ages.
- Poisson's coefficient (EN 12390-13 [67]) at 28 and 90 days in three cylindrical specimens (same specimens as those used for the elastic-modulus test).
- Splitting tensile strength (EN 12390-6 [68]) at 28 days in three cylindrical specimens.
- Flexural strength (EN 12390-5 [69]) at 28 days in three prismatic specimens.

3. Results and Discussion

3.1. Fresh Performance

3.1.1. Slump-Flow Test

The slump flows of the SCC mixes are plotted in Figure 7a, and the t_{500} times in Figure 7b. These parameters define the flowability and flow speed of SCC under free flow, respectively. In slump-flow terms, the *RW* mix was of SF2 slump-flow class, while the *W*1.5 and *W*3.0 mixes were of SF1 class [61]. All the mixes were of VS2 class.

The decreasing slump flow of SCC when adding RCWTB (variations of -14.2% and -21.3% for the *W*1.5 and *W*3.0 mixes, respectively) were because this waste increased the specific surface area of the SCC components. The GFRP fibers and micro-fibers had a high surface area [38], as can be noted in Figure 4, while the balsa-wood particles exhibited a high surface porosity [70]. This phenomena in turn resulted in a reduction of the free water in the SCC, which increased the internal friction among all their components [14], thus reducing the ability of the cement paste to drag all of them uniformly. However, it should be noted that the increased water/cement ratio partially compensated such performance,

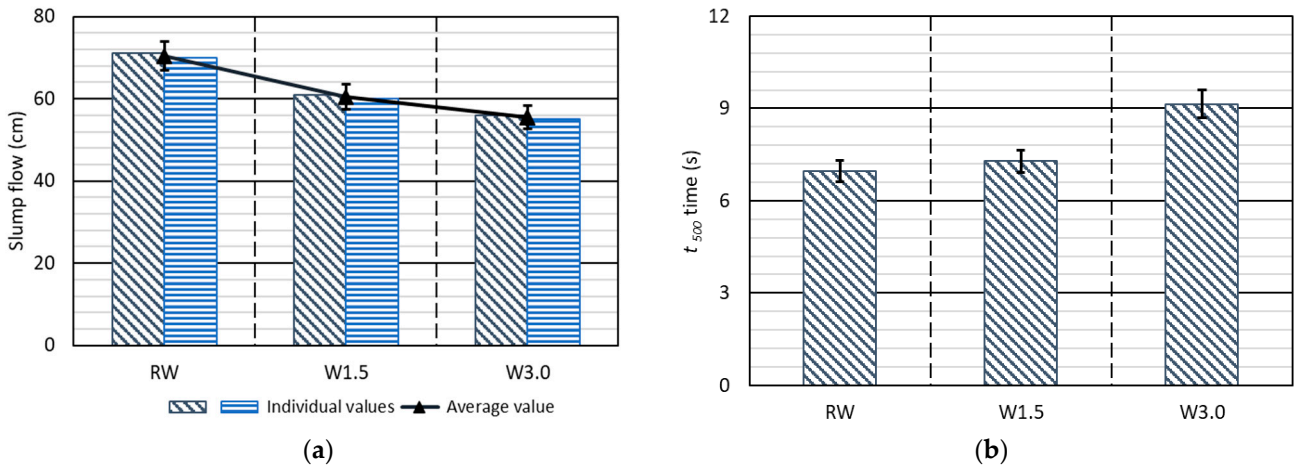so this negative trend could have been more pronounced if no water compensation had been conducted [39].

Figure 7. Experimental results of the slump-flow test: (**a**) slump flow; (**b**) t_{500} time.

The t_{500} time increased with the addition of RCWTB, although the variation was not as linear with the RCWTB content as in the case of slump flow. The increase in time between the *RW* and W1.5 mixes was only about 0.3 s, while the increase between the reference SCC mix and W3.0 mix was 2.2 s (31.3% increase). In view of this behavior, it appears that the negative effect of the addition of 1.5% RCWTB occurred primarily when SCC reached a high slump flow, since it did not affect the time that SCC took to reach a reduced slump flow of 500 mm. This behavior has also been found for other alternative raw materials [19,26] and can be explained by the ability of the cement paste to maintain adequate cohesion between all SCC components at low slump-flow levels [6]. This was also reflected in the low sieve-segregation values achieved (EN 12350-11 [71]), less than 4% in all the SCC mixtures regardless of the RCWTB content.

As a consequence of the slightly different trends shown by both slump flow and t_{500} time, the two properties did not have a very close linear dependence, as shown in Figure 8. This indicates that the free flow of SCC containing RCWTB does not occur at a uniform rate over time, especially when this waste is used at a content of 1.5%.
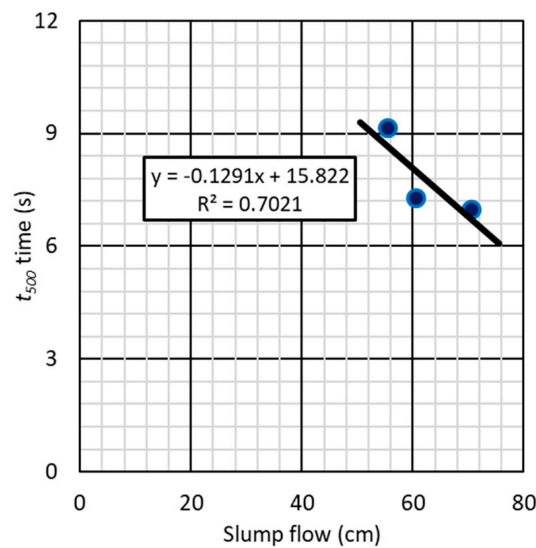

Figure 8. Relationship (linear simple regression) between the results of the slump-flow test.

3.1.2. 3-Bar L-Box Test

The 3-bar L-box blocking ratio was calculated as the quotient between SCC height at the end of the horizontal flow area and before the gate when SCC movement finished. The results obtained are shown in Figure 9. Only the *RW* mix reached the minimum value required of 0.80 to establish an L-box class to SCC, so a PA2 class could only be assigned to this SCC mix [61]. Therefore, it is clear that the RCWTB interfered with the motion of the other SCC components under such flow conditions [72], even when this residue was added in small amounts, as the *W*1.5 mix showed a 3-bar L-box blocking ratio 18.5% lower than that of the reference mix. When RCWTB was added in a content of 3.0%, the decrease in the blocking ratio increased to 42.9%.
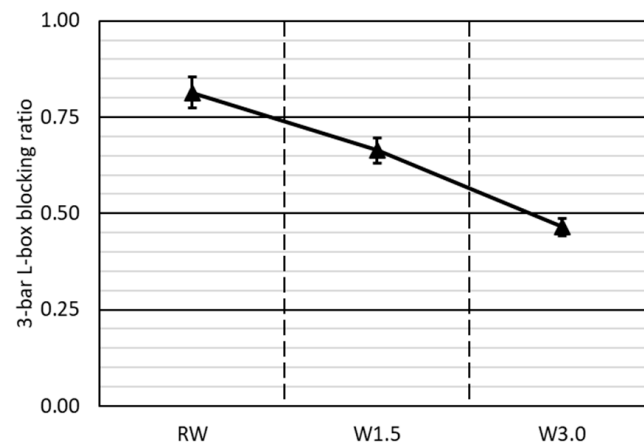

Figure 9. Experimental results of the 3-bar L-box test: blocking ratio.

It follows from these results that the impact of RCWTB on the L-box passing ability of SCC was much more noticeable and negative than in terms of free flow (Figure 7), which is thought to be primarily because of the effect of the GFRP fibers. As other types of commercial fibers in SCC, they were trapped between the bars that simulate the concrete reinforcement [28,46]. Therefore, fibers generally require a denser cement paste in SCC to be able to successfully drag them through the bars of the testing apparatus.

3.1.3. 16-Bar J-Ring Test

The values of the slump flow, t_{500} time, and blocking ratio, obtained in the 16-bar J-ring test, are shown in Figure 10.

The results regarding slump flow (Figure 10a) and t_{500} time (Figure 10b) were affected by the presence of obstacles simulating concrete reinforcement, which hindered SCC flow [4]. Therefore, slump flows obtained in this test were lower than in the slump-flow test. Furthermore, only the *RW* and *W*1.5 mixes were of J-ring SF1 class, as the *W3.0* mix did not reach the minimum required value of 550 mm [61]. Similarly, the t_{500} times were higher than in the slump-flow test, with all mixes being J-ring VS2 class. On the other hand, the results of the 16-bar J-ring test corroborated the trends regarding the effect of increasing the amount of RCWTB in SCC found in the slump-flow test. An amount of 1.5% RCWTB caused a notable decrease in the slump flow (14.4% loss), while the increase in the t_{500} time that it caused was only 3.4%. These percentage variations for the *W3.0* mix were 21.6% and 30.9%, respectively. Therefore, the reduction in the free water [46] and the subsequent increase in the internal friction between the SCC components [14] due to the addition of low RCWTB content only notably affected the free flow of the mixtures when high slump-flow values were reached, even despite the presence of bars simulating concrete reinforcement, such as in the J-ring test.
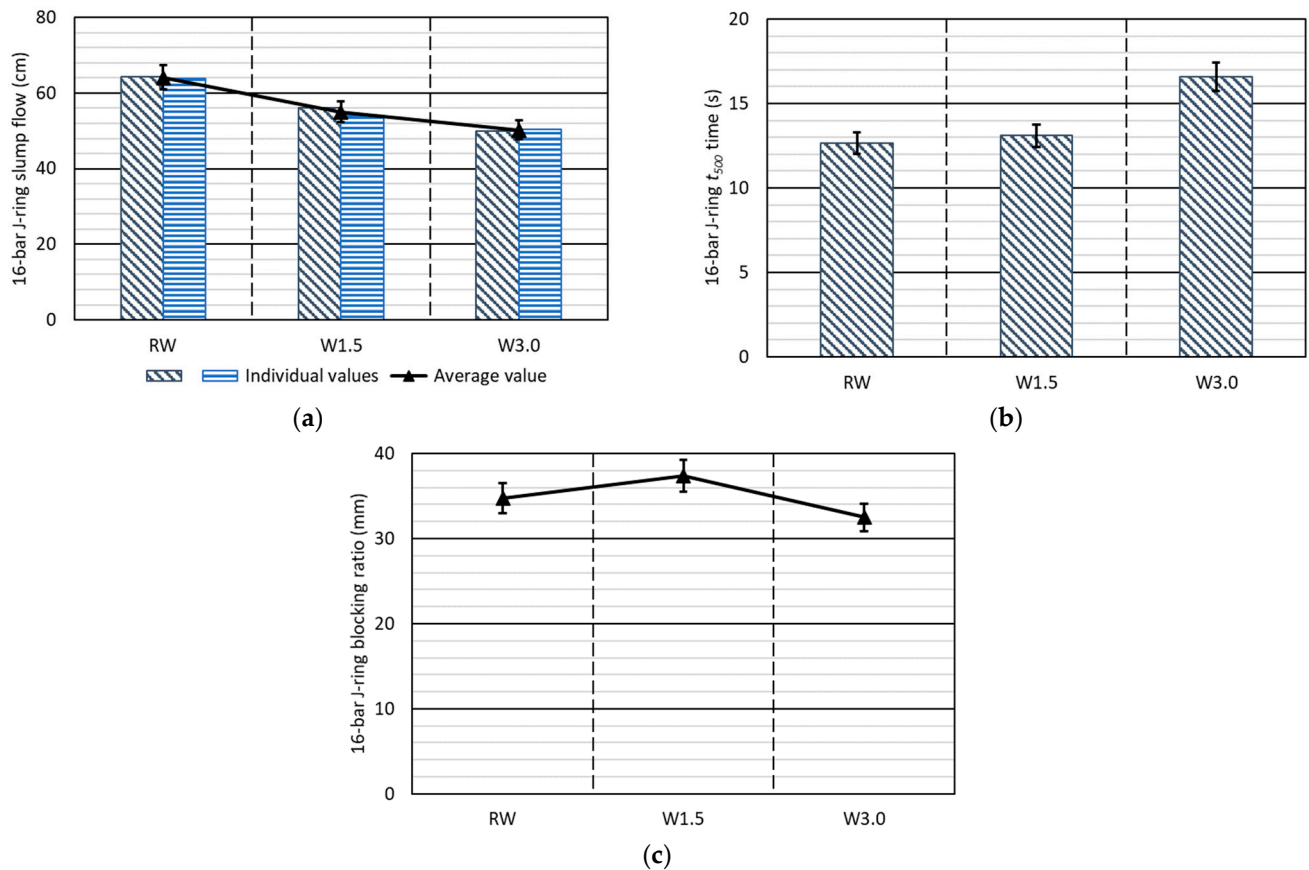
(a)

(b)

(c)

Figure 10. Experimental results of the 16-bar J-ring test: (**a**) slump flow; (**b**) t_{500}; (**c**) blocking ratio.

The J-ring blocking ratio (Figure 10c) was measured as the difference in SCC height between the center and the outside of the ring when SCC movement ended [61]. This value remained approximately constant among the three SCC mixtures, with results between 32.5 mm (*W*3.0 mix) and 37.0 mm (*W*1.5 mix). RCWTB did not impact SCC passing ability under free flow, as it is thought that the cement paste could successfully drag the GFRP fibers through the bars of the J-ring. Other research has also reported such phenomena regarding different types of fibers [28,72].

The relationships between the different results of the 16-bar J-ring test corroborated all the aspects mentioned above, as can be seen in Figure 11. No precise linear relationship was detected between the t_{500} time and the slump flow, as regarding the slump-flow test (Figure 8). Similarly, the blocking ratio did not show a clear dependence with the other two properties, although this relationship was slightly more precise with the t_{500} time.

3.1.4. Inter-Test Relationships

Figure 12 details the inter-relationships (linear simple regressions) between the results obtained in the different fresh tests. It can be appreciated that slump flows and t_{500} times obtained in the slump-flow and 16-bar J-ring tests showed proportional values, indicating that the free-flow results of SCC containing RCWTB exhibited the same trends with and without the presence of obstacles. However, the trend of the blocking ratios depended on whether SCC flowed in an imposed direction (3-bar L-box test) or whether it flowed under free-flow conditions (16-bar J-ring test). Therefore, a non-precise relationship between them was detected (Figure 12c). It is suggested that the cement paste was able to drag them more easily and successfully under free-flow conditions, which are generally the most favorable for SCC movement [42,73].
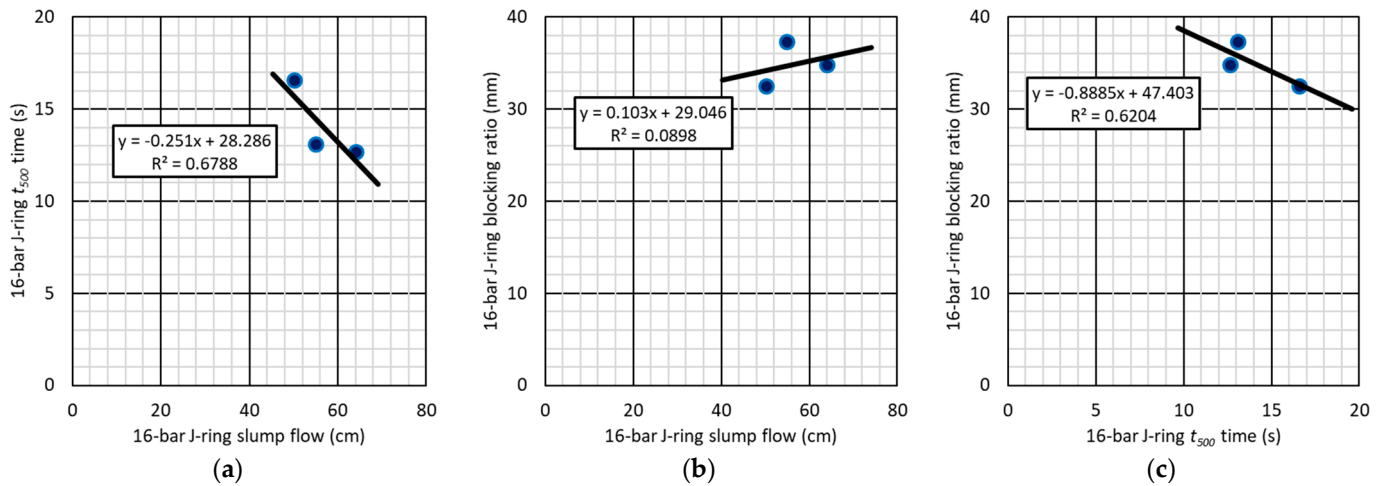
Figure 11. Relationships (linear simple regression) between the results of the 16-bar J-ring test: (**a**) slump flow and t_{500} time; (**b**) slump flow and blocking ratio; (**c**) t_{500} time and blocking ratio.
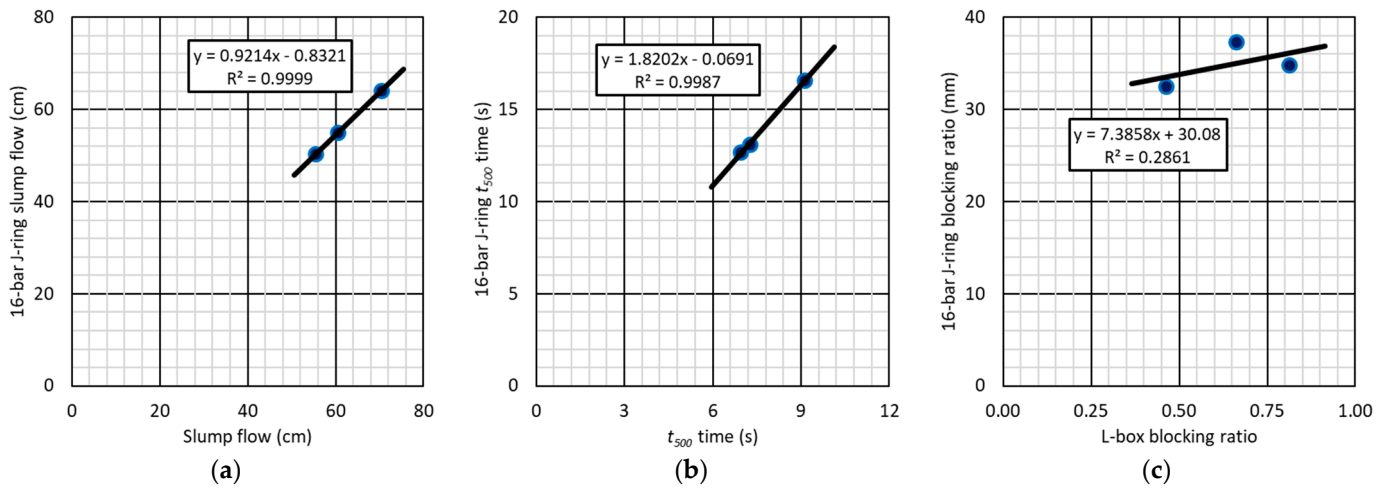

Figure 12. Inter-relationships (linear simple regression) between the results of the different fresh SCC tests: (**a**) slump flow; (**b**) t_{500} time (**c**) blocking ratio.

3.1.5. Statistical Validation

To conclude the evaluation of the experimental results related to the fresh behavior of SCC containing RCWTB, two statistical analyses were performed. On the one hand, the significance of the factor "RCWTB content" was analyzed for all the properties by means of a one-way analysis of variance (ANOVA) at a significance level of 5%. On the other hand, both linear (Pearson) and monotonic (Spearman) correlations between the RCWTB content and all the fresh properties were determined. All these analyses are common in concrete science [74,75]. The results obtained are shown in Table 4.

Table 4. *p*-Values for the one-way ANOVA and correlations of the experimental fresh results.

Test	Parameter	*p*-Value	Pearson's Correlation	Spearman's Correlation
Slump-flow test	Slump flow	0.0010	−0.98	−0.95
	t_{500} time	0.0005	+0.92	+0.96
3-bar L-box test	Blocking ratio	0.0001	−1.00	−0.98
	Slump flow	0.0009	−0.98	−0.96
16-bar J-ring test	t_{500} time	0.0005	+0.91	+0.93
	Blocking ratio	0.0603	−0.46	−0.48

The RCWTB content significantly affected all the fresh-SCC properties, as *p*-values markedly lower than 0.05 were obtained [74]. The only exception was the blocking ratio of the 16-bar J-ring test, as the content of this waste did not significantly affect it. The correlations were consistent with the findings of the one-way ANOVA, the RCWTB content having a close relationship with all properties since the absolute values of the correlations were greater than 0.90. The exception once again was the blocking ratio obtained in the 16-bar J-ring test. The correlations also showed that all properties decreased with the RCWTB amount (negative sign), except for the t_{500} time, which increased (positive sign).

3.2. CFD Simulations

3.2.1. Adjustment of Bingham Equation Through the Slump-Flow Test

The values of the Bingham parameters τ_0 and μ were obtained through iterative simulations based on the experimental results of the slump-flow test, as shown in Figure 13. In each iteration, a different value of both parameters was assigned until the results of the simulation of the slump-flow test coincided with those experimentally obtained. The initial values for the iterations were defined according to similar research [46,50,63,64].
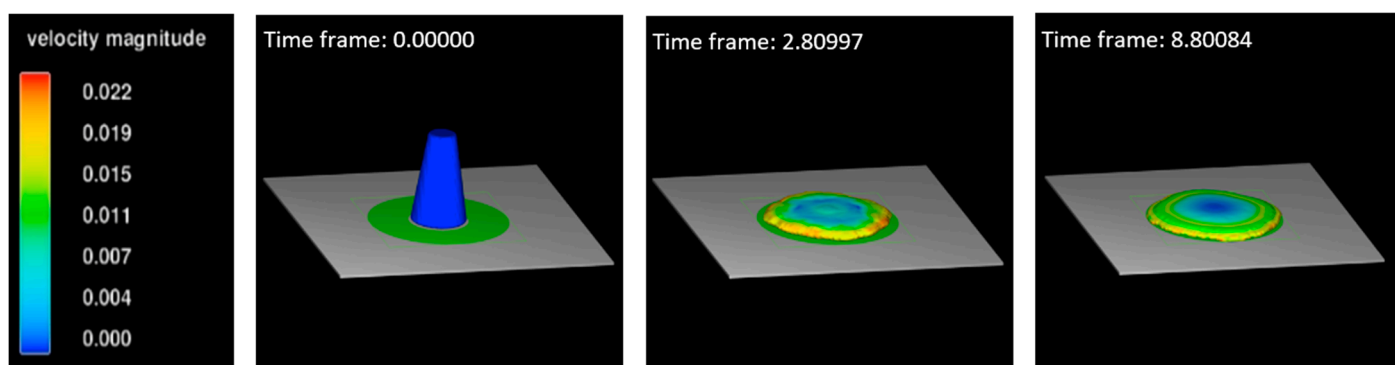

Figure 13. Example of the simulation of the slump-flow test in the *RW* mix.

The values obtained for both parameters yield stress and plastic viscosity, allowed for defining by the Bingham equation (Equation (1)) for each SCC mixture, as shown in Figure 14a. Such parameters also allowed for defining the viscosity law of each SCC mix (Equation (2)), which are detailed in Figure 14b. Two aspects can be highlighted from the results achieved through CFD simulations:

- The addition of RCWTB did not affect yield stress (Figure 14a), with all SCC mixes showing a similar value around 120 Pa. Therefore, SCC with contents of this waste up to 3.0% started to freely flow at the same shear stress. This could be expected in view of the t_{500}-time results obtained in the slump-flow and 16-bar J-ring tests, where 1.5% RCWTB did not affect the free flow of SCC at low slump-flow levels (Figures 7b and 10b). This means that the start of SCC free flow always happened under the same initial conditions (yield stress) regardless of the RCWTB content [63].
- However, RCWTB did noticeably affect the value of the SCC plastic viscosity (Figure 14a). The addition of 1.5% RCWTB increased the viscosity by around 3.5 times (116 Pa·s vs. 429 Pa·s), although higher waste amounts did not result in such a large increase, as the viscosity of the *W3.0* mix was 517 Pa·s. The GFRP fibers exhibited a hard movement against shear stresses and also increased the solid concentration within SCC, which hindered the flow of the aggregate particles progressively as the slump flow of the SCC increased [9,28]. The same phenomena have been found when adding other fiber types to SCC, their long-term effect being more negative than that at the beginning of the free flow [72]. These effects also caused the stabilization of the apparent viscosity to occur at lower shear rates, as can be noted in Figure 14b.
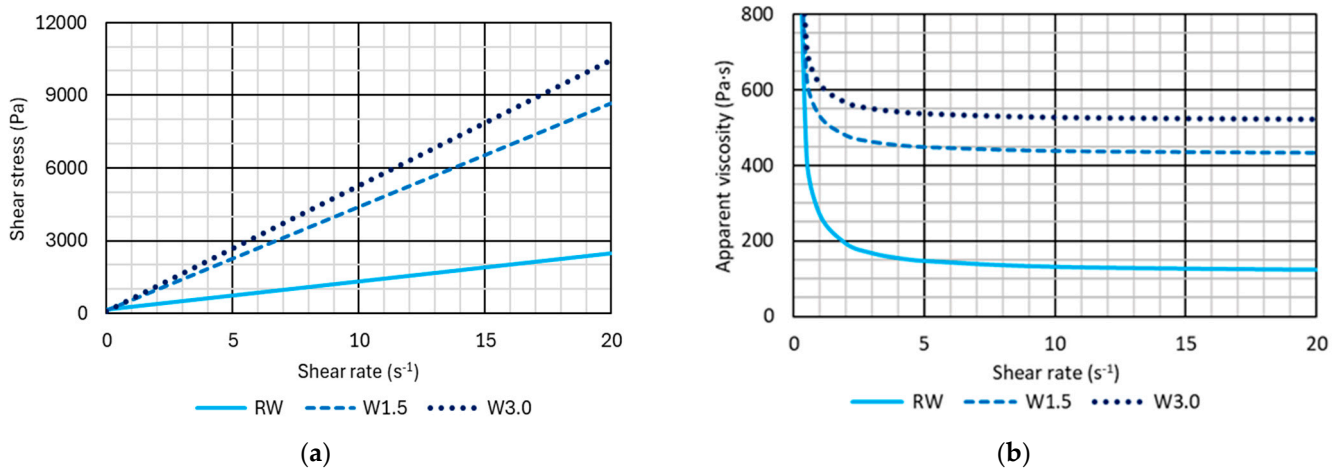
Figure 14. CFD simulation of the slump-flow test: (**a**) Bingham equation; (**b**) viscosity law.

Figure 15 shows the relationship based on simple linear regression between the plastic viscosity obtained from CFD simulations and the results of the slump-flow test. It can be seen that the viscosity exhibited a very close relationship with the slump flow, while the relationship with the t_{500} time had a much lower R^2 coefficient. These statistical relationships support the aspects discussed above. The plastic viscosity conditioned the free-flow behavior of SCC containing RCWTB in the long term, allowing to accurately explain the value of the slump flow, measured when SCC movement ended. However, it was not as successful in explaining the behavior of SCC with RCWTB at the beginning of the free flow, when the negative effect of RCWTB was less noticeable.
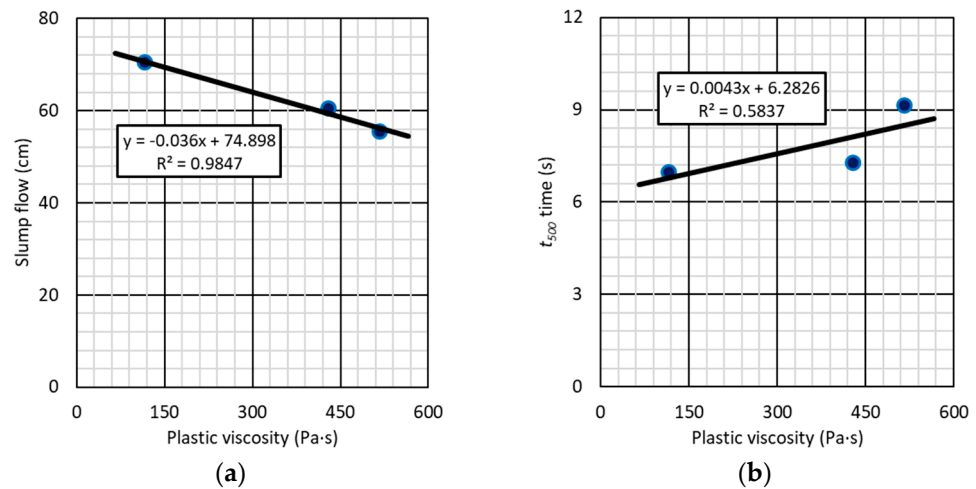

Figure 15. Linear simple regression between plastic viscosity and: (**a**) slump flow; (**b**) t_{500} time.

3.2.2. Simulation of the 3-Bar L-Box Test

Once adjusted using the Bingham equation (Figure 14), the L-box test was simulated, as shown in Figure 16. The error rates for the blocking ratio derived from this test are listed in Table 5.

Table 5. Error rates from the CFD simulation of the blocking ratio from the 3-bar L-box test.

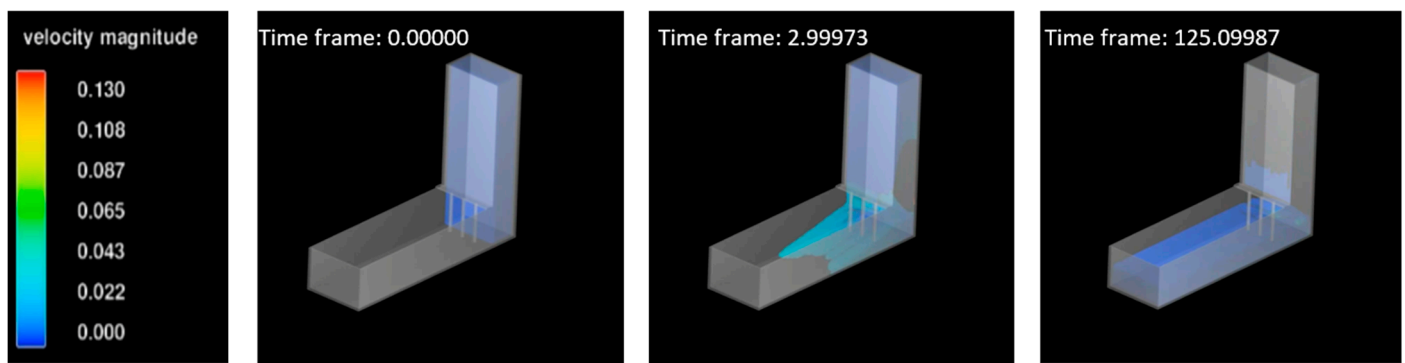| Mix	Error Rate (%)
RW	20.5
W1.5	48.2
W3.0	107.4

Figure 16. Example of the simulation of the 3-bar L-box test in the *W*1.5 mix.

The CFD simulations adjusted the blocking ratio from the 3-bar L-box test more accurately the lower the content of RCWTB and, therefore, of the GFRP fibers in SCC. Thus, the error rate went from 20.5% in the *RW* mix to 107.4% in the *W*3.0 mix. CFD simulations always obtained higher blocking ratios than the experimental ones and, therefore, a better SCC flow under these conditions. This behavior could be due to the fact that the CFD simulations did not allow for introducing the individual effect of the GFRP fibers [63], which are thought to be partially retained in the bars simulating concrete reinforcement, which hindered the SCC flow. The plastic viscosity did not show a poor relationship with the experimental results of the 3-bar L-box blocking ratio, as can be seen in Figure 17. Therefore, it is considered that the Bingham parameters obtained were also in agreement with the results of the 3-bar L-box test, although the simulation of the individual effect of the GFRP fibers would provide greater accuracy [48]. On the other hand, the use of smaller meshes could also improve the simulation accuracy [46].
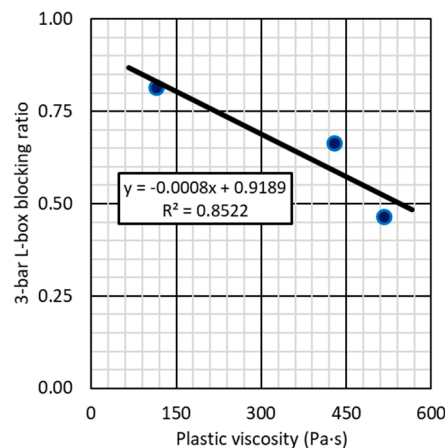

Figure 17. Linear simple regression between plastic viscosity and 3-bar L-box test.

3.2.3. Simulation of the 16-Bar J-Ring Test

The 16-bar J-ring test was also simulated through CFD tools by considering the parameters of the Bingham equation obtained from the results of the slump-flow test (Figure 14), as shown in Figure 18. The error rates for the different results of the tests are listed in Table 6.

Table 6. Error rates (%) of the CFD simulation of the 16-bar J-ring test.

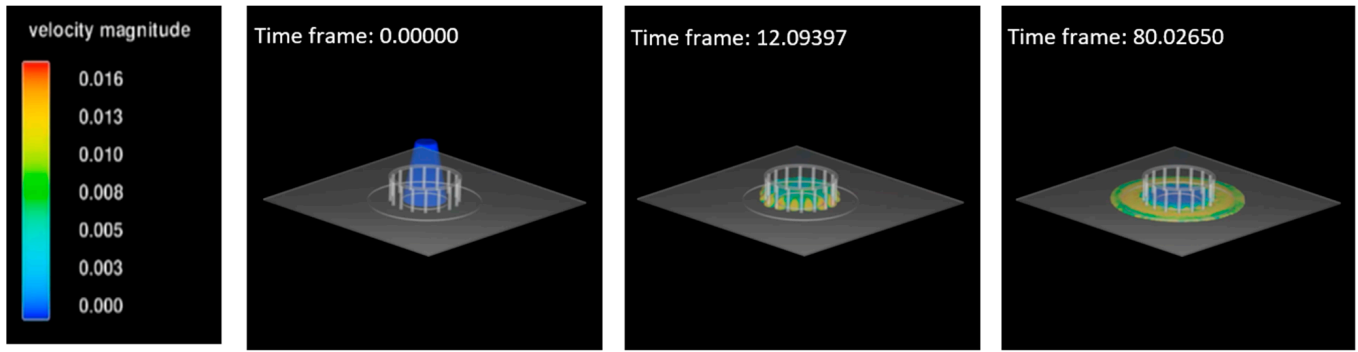| Mix	Slump Flow	t_{500} Time	Blocking Ratio
RW	5.1	10.5	55.2
*W*1.5	12.7	14.5	72.1
*W*3.0	22.8	32.7	62.1

Figure 18. Example of the simulation of the J-ring test in the *W3.0* mix.

The results obtained in this test were modeled with varying accuracy by means of CFD tools. Thus, two different groups could be distinguished depending on the fitting quality:

- On the one hand, there are slump flow and t_{500} time. The error rate for these results was higher with the RCWTB content. For example, the error rate of the 16-bar J-ring slump flow was 5.1% of the *RW* mixture and 10.5% for its t_{500} time, while these values for the *W3.0* mix were 22.8% and 32.7%, respectively. Nevertheless, these values were always within adequate limits according to the indications of other studies available in the scientific literature [63,64], thus validating the adjustment of the Bingham equation conducted and the CFD model developed through the results of the slump-flow test. As for the slump-flow test (Figure 15), a more precise relationship of the plastic viscosity with the slump flow (Figure 19a) than with the t_{500} time (Figure 19b) was found. The plastic viscosity thus enabled us to explain and successfully simulate the free flow of SCC containing RCWTB in the long term regardless of the presence of obstacles simulating concrete reinforcements, which is in line with the trends found in other studies [46].

- On the other hand, the error rates obtained for the blocking ratio were high, in all cases greater than 55%. No clear trend with the RCWTB amount was found, nor a precise relationship with the plastic viscosity (Figure 19c). This property did not depend on the Bingham parameters, and the GFRP fibers may have a much more noticeable influence that could be further explored by other simulation approaches [48] or by considering meshes of lower size [46].
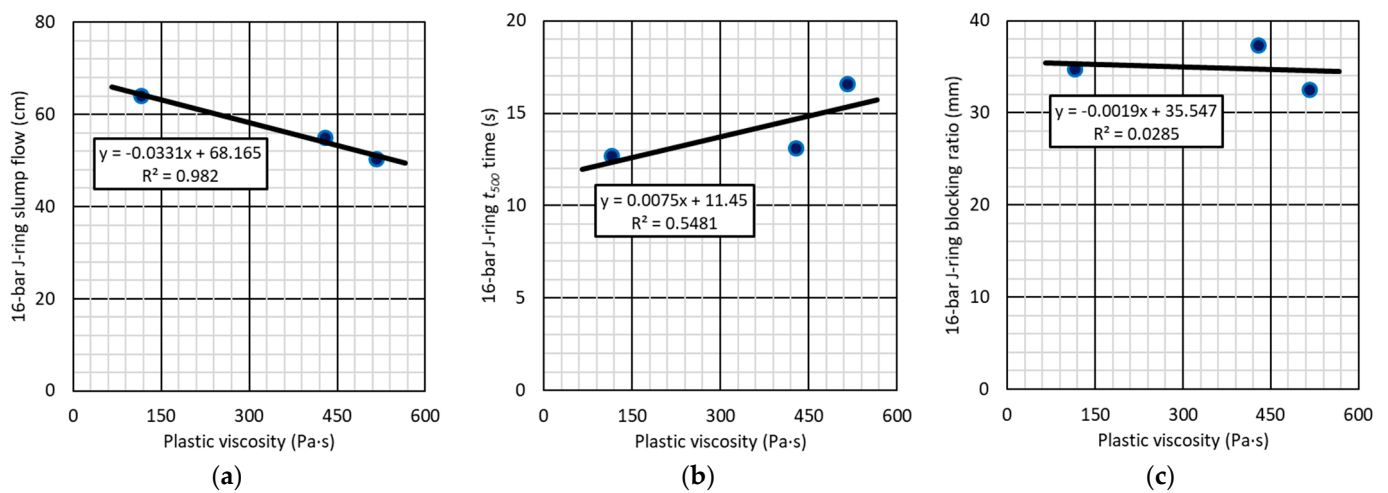

Figure 19. Relationship (linear simple regression) between plastic viscosity and 16-bar J-ring test: (**a**) slump flow; (**b**) t_{500} time; (**c**) blocking ratio.

3.2.4. Statistical Validation

As for the experimental results in the fresh state, the impact of the RCWTB content on the parameters of the Bingham model, yield stress, and plastic viscosity was validated through a one-way ANOVA at a 5% significance level and by calculating Pearson's and Spearman's correlations. The results obtained are detailed in Table 7. These results show that the RCWTB content did not affect the yield stress of SCC, which resulted in very low correlations. However, the plastic viscosity was significantly affected by the content of this residue in SCC, which led to high correlation values, especially in linear terms.

Table 7. *p*-Values for the one-way ANOVA and correlations of the CFD simulations.

Parameter	*p*-Value	Pearson's Correlation	Spearman's Correlation
Yield stress	0.0789	−0.51	−0.54
Plastic viscosity	0.0111	+0.93	+0.84

3.3. Mechanical Properties

3.3.1. Experimental Results

The values of the mechanical properties are plotted in Figure 20. The compression-related properties were determined at early ages and advanced ages apart from at 28 days. Splitting tensile and flexural strengths were also measured at 28 days.

The trends displayed by all the mechanical properties with the content of RCWTB were similar except for Poisson's coefficient. Therefore, all of them decreased in an approximately linear way as the RCWTB amount increased. This performance is thought to be due to two aspects. First, the weak particles of polymers and balsa wood that were introduced within the SCC when RCWTB was used as a raw material. They created interfacial transition zones with low levels of adhesion to the cementitious matrix, which could have caused these particles to slide when loading, as found for other concrete types [76]. Furthermore, they could easily break when applying the load in those cases in which they exhibited a better adhesion to the cementitious matrix [56,70]. Second, the large increase in the water/cement ratio as the RCWTB content was augmented to preserve self-compactability in terms of free flow without obstacles [11]. These trends were not affected by age, as the 7-day compressive strength and compression-related mechanical properties at 90 days exhibited equivalent trends. These aspects caused the *W*3.0 mix not to show mechanical properties with values suitable for use in structural applications [77].

GFRP fibers show optimal adhesion to the cementitious matrix due to the wedge effect created between the matrix and the fiberglass in the interfacial transition zone, which causes the cementitious matrix to break instead of slipping [76]. Nevertheless, the stitching effect of the GFRP fibers was largely counterbalanced by the two aspects mentioned in the previous paragraph. Thus, these fibers did not contribute to the improvement of the mechanical properties of SCC, unlike what was found in conventional-workability concrete [41]. Only Poisson's coefficient was positively affected by them, since their stitching effect limited the transverse deformability [39], causing this property to remain constant for all SCC mixes regardless of the RCWTB content.

From the results of these mechanical properties, it can be concluded that it is necessary to develop an SCC design specifically aimed not only to achieve self-compacting properties when RCWTB is added, but to ensure that adequate mechanical behavior is achieved. The study of varying the content of superplasticizers [78], the use of filler to improve the density of the fresh cement paste and the mechanical strength when hardened [5], and the analysis of other possible ways of adding RCWTB as, for instance, an aggregate replacement [34], are strategies that can be applied in future research. Another possibility would be to obtain higher quality GFRP fibers as in other studies in the literature [39], or that those fibers were not mixed with weak particles of balsa wood and polymers. This may enable the addition of waste from wind-turbine blades to SCC to yield a better mechanical performance.
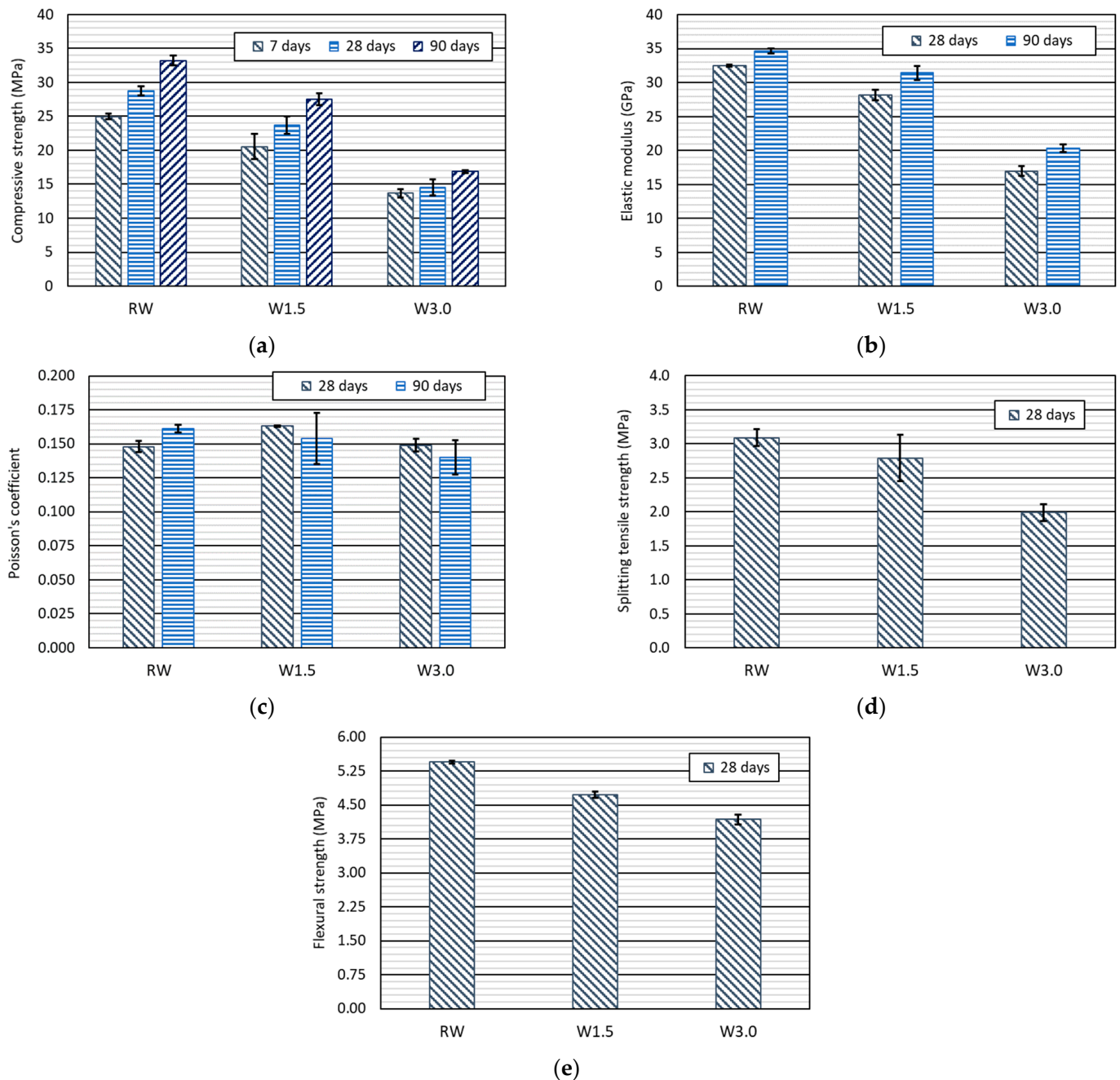
Figure 20. Mechanical properties of the SCC mixes: (**a**) compressive strength; (**b**) elastic modulus; (**c**) Poisson's coefficient; (**d**) splitting tensile strength; (**e**) flexural strength.

3.3.2. Statistical Validation

The significance of the RCWTB content on the mechanical properties of SCC was verified in the same way as in the previous cases, through a one-way ANOVA with a significance level of 5%, and by calculating the correlations between the content of this residue and the values of the mechanical properties. As shown in Table 8, the effect of RCWTB was significant in all mechanical properties except Poisson's coefficient. In fact, negative correlations of high absolute value were obtained in all these cases, both linear (Pearson) and monotonic (Spearman), which confirmed the negative relevance of the amount of RCWTB in the results of the mechanical properties [75]. As expected, the correlations for Poisson's coefficient had very low absolute values.

Table 8. *p*-Values for the one-way ANOVA and correlations of the mechanical properties.

Property	Age (Days)	*p*-Value	Pearson's Correlation	Spearman's Correlation
Compressive strength	7	0.0030	−0.92	−0.95
	28	0.0005	−0.95	−0.95
	90	0.0000	−0.97	−0.95
Modulus of elasticity	28	0.0000	−0.96	−0.95
	90	0.0000	−0.94	−0.95
Poisson's coefficient	28	0.0865	+0.05	+0.05
	90	0.6696	−0.34	−0.51
Splitting tensile strength	28	0.0404	−0.77	−0.74
Flexural strength	28	0.0009	−0.95	−0.95

4. Conclusions

The crushing of wind-turbine blades to produce raw-crushed wind-turbine blade (RCWTB) and its addition to self-compacting concrete (SCC) is a possible way to recycle these wind-turbine components. This contributes to the circular economy in the wind sector and to the revaluation of material that currently has no added value. This paper has presented a first approach for the use of RCWTB as a raw material in SCC production following a conventional design. These conclusions can be drawn from all the aspects discussed:

- RCWTB decreased the flowability of the SCC under free-flow conditions, reducing slump flow and increasing t_{500} time. This behavior was independent of the presence (16-bar J-ring test) or not (slump-flow test) of obstacles simulating concrete reinforcement. An amount of 1.5% RCWTB content yielded SCC with proper fresh behavior under free flow, while an amount of 3.0% RCWTB was excessive to obtain SCC with proper flowability in the 16-bar J-ring test.
- The passing ability of SCC was affected differently by RCWTB depending on the type of flow imposed. Thus, this property was not affected under free-flow conditions (16-bar J-ring test). However, any RCWTB content led to a very noticeable decrease of the blocking ratio when flow was imposed in a specific direction (3-bar L-box test). It is thought that the fibers of glass fiber-reinforced polymer (GFRP) present in this waste may have been retained by the bars simulating concrete reinforcement in this test, hindering the passage of SCC.
- Obtaining the Bingham parameters based on the results of the slump-flow test by computational fluid dynamics (CFD) simulations showed that RCWTB did not affect the yield stress of SCC, but it did significantly increase the plastic viscosity. Thus, SCC started to flow freely under the same shear stress regardless of the waste content, but RCWTB did slow down the flow, especially in the long term.
- The CFD simulation based on the Bingham model was valid for free flow, both with and without obstacles simulating concrete reinforcement, obtaining valid differences with the experimental results. This simulation was more suitable for long-term flow, since slump flow was always simulated more accurately than t_{500} time.
- CFD tools did not allow accurate modeling of the passing ability of SCC, although the plastic viscosity obtained did exhibit a good relationship with the 3-bar L-box blocking ratio. Modeling the effect of the GFRP fibers on SCC flow could improve the accuracy of the simulation.
- The addition of RCWTB worsened all mechanical properties due to the presence of polymer and balsa-wood particles and to the increase of the water/cement ratio with increasing contents of this waste. Moreover, these aspects offset the beneficial effect of stitching the GFRP fibers, which was only relevant in terms of Poisson's coefficient, which remained constant for all RCWTB content. The mix with 3.0% RCWTB did not exhibit adequate mechanical properties for use in structural elements.

From all the aspects analyzed, it can be concluded that it is possible to develop SCC through the addition of RCWTB that exhibits adequate free-flow behavior, both in experimental and CFD-simulation terms. The direct comparison of experimental results with CFD-simulation outputs could be addressed in future research. Despite this, it is also true that a conventional SCC design is not suitable. It is therefore necessary to develop a specific dosage for SCC incorporating this residue, so that high content of this waste can be added without reducing so notably the passing ability and mechanical properties of SCC. This is an aspect that could be addressed in future research, as well as the use of GFRP fibers of higher quality to produce SCC.

Author Contributions: Conceptualization, M.H.-R. and V.R.-C.; methodology, V.R.-C. and V.O.-L.; software, M.H.-R. and V.R.-C.; validation, J.A.C. and J.M.M.; formal analysis, M.H.-R. and V.R.-C.; investigation, M.H.-R. and V.R.-C.; resources, V.O.-L. and J.M.M.; data curation, M.H.-R. and V.R.-C.; writing—original draft preparation, M.H.-R. and V.R.-C.; writing—review and editing, J.A.C., V.O.-L. and J.M.M.; visualization, J.A.C., V.O.-L. and J.M.M.; supervision, J.A.C., V.O.-L. and J.M.M.; project administration, V.O.-L. and J.M.M.; funding acquisition, V.O.-L. and J.M.M. All authors have read and agreed to the published version of the manuscript.

Institutional Review Board Statement: Not applicable.

Informed Consent Statement: Not applicable.

Data Availability Statement: The raw data supporting the conclusions of this article will be made available by the authors upon request.

Conflicts of Interest: Author José A. Chica was employed by the company TECNALIA. The remaining authors declare that the re-search was conducted in the absence of any commercial or financial relationships that could be construed as a potential conflict of interest.

References

1. Okamura, H. Self-compacting high-performance concrete. *Concr. Int.* **1997**, *19*, 50–54.
2. Ghorbani, A.; Maleki, H.; Naderpour, H.; Khatami, S.M.H. Advancing Compressive Strength Prediction in Self-Compacting Concrete via Soft Computing: A Robust Modeling Approach. *J. Soft Comput. Civ. Eng.* **2024**, *8*, 126–140. [CrossRef]
3. Nasr, M.S.; Salman, A.J.; Ghayyib, R.J.; Shubbar, A.; Al-Mamoori, S.; Al-khafaji, Z.; Hashim, T.M.; Hasan, Z.A.; Sadique, M. Effect of Clay Brick Waste Powder on the Fresh and Hardened Properties of Self-Compacting Concrete: State-of-the-Art and Life Cycle Assessment. *Energies* **2023**, *16*, 4587. [CrossRef]
4. Malazdrewicz, S.; Adam Ostrowski, K. Self-compacting concrete with recycled coarse aggregates from concrete construction and demolition waste—Current state-of-the art and perspectives. *Constr. Build. Mater.* **2023**, *370*, 130702. [CrossRef]
5. Revilla-Cuesta, V.; Fiol, F.; Perumal, P.; Ortega-López, V.; Manso, J.M. Using recycled aggregate concrete at a precast-concrete plant: A multi-criteria company-oriented feasibility study. *J. Clean. Prod.* **2022**, *373*, 133873. [CrossRef]
6. Nepomuceno, M.C.S.; Pereira-De-Oliveira, L.A.; Lopes, S.M.R. Methodology for the mix design of self-compacting concrete using different mineral additions in binary blends of powders. *Constr. Build. Mater.* **2014**, *64*, 82–94. [CrossRef]
7. Nepomuceno, M.C.S.; Pereira-De-Oliveira, L.A.; Lopes, S.M.R.; Franco, R.M.C. Maximum coarse aggregate's volume fraction in self-compacting concrete for different flow restrictions. *Constr. Build. Mater.* **2016**, *113*, 851–856. [CrossRef]
8. Devi, K.; Aggarwal, P.; Saini, B. Admixtures Used in Self-Compacting Concrete: A Review. *Iran. J. Sci. Technol. Trans. Civ. Eng.* **2020**, *44*, 377–403. [CrossRef]
9. Ortega-López, V.; García-Llona, A.; Revilla-Cuesta, V.; Santamaría, A.; San-José, J.T. Fiber-reinforcement and its effects on the mechanical properties of high-workability concretes manufactured with slag as aggregate and binder. *J. Build. Eng.* **2021**, *43*, 102548. [CrossRef]
10. Ahmad, J.; Zhou, Z.; Deifalla, A.F. Self-Compacting Concrete with Partially Substitution of Waste Marble: A Review. *Int. J. Concr. Struct. Mater.* **2023**, *17*, 25. [CrossRef]
11. Pereira-de Oliveira, L.A.; Nepomuceno, M.; Rangel, M. An eco-friendly self-compacting concrete with recycled coarse aggregates. *Inf. Constr.* **2013**, *65*, 31–41. [CrossRef]
12. Kohandelnia, M.; Hosseinpoor, M.; Yahia, A.; Belarbi, R. Multiscale investigation of self-consolidating earthen materials using a novel concrete-equivalent mortar approach. *Constr. Build. Mater.* **2023**, *370*, 130700. [CrossRef]

13. Kohandelnia, M.; Hosseinpoor, M.; Yahia, A.; Belarbi, R. New insight on rheology of self-consolidating earth concrete (SCEC). *Powder Technol.* **2023**, *424*, 118561. [CrossRef]

14. Caracol, C.; Kravchanka, L.; Bravo, M.; de Brito, J.; Agrela, F.; Rosales, J. Recycled aggregate concrete using seawater: Optimizing concrete's sustainability. *J. Build. Eng.* **2024**, *97*, 110841. [CrossRef]

15. Faleschini, F.; Jiménez, C.; Barra, M.; Aponte, D.; Vázquez, E.; Pellegrino, C. Rheology of fresh concretes with recycled aggregates. *Constr. Build. Mater.* **2014**, *73*, 407–416. [CrossRef]

16. Brand, A.S.; Fanijo, E.O. A review of the influence of steel furnace slag type on the properties of cementitious composites. *Appl. Sci.* **2020**, *10*, 8210. [CrossRef]

17. Santamaría, A.; Orbe, A.; Losañez, M.M.; Skaf, M.; Ortega-Lopez, V.; González, J.J. Self-compacting concrete incorporating electric arc-furnace steelmaking slag as aggregate. *Mater. Des.* **2017**, *115*, 179–193. [CrossRef]

18. Tran, T.Q.; Kim, Y.S.; Dang, L.C.; Do, T.M. A state-of-the-art review on the utilization of new green binders in the production of controlled low-strength materials. *Constr. Build. Mater.* **2023**, *393*, 132078. [CrossRef]

19. Busari, A.A.; Akinmusuru, J.O.; Dahunsi, B.I. Review of sustainability in self-compacting concrete: The use of waste and mineral additives as supplementary cementitious materials and aggregates. *Port. Electrochim. Acta* **2018**, *36*, 147–162. [CrossRef]

20. Kushefati, W.H.; Abubakar, A.B.; Farhan, K.Z. Influence of fineness modulus of fine aggregates on mechanical and thermal resistance properties of alkali-activated slag composites. *Innov. Infrastruct. Solut.* **2024**, *9*, 268. [CrossRef]

21. Metla, M.N.A.; Amin, M.N.; Rizwan, S.A.; Khan, K. Self-consolidating paste systems using ground granulated blast furnace slag and limestone powder mineral admixtures. *Case Stud. Constr. Mater.* **2024**, *20*, e03316. [CrossRef]

22. Revilla-Cuesta, V.; Skaf, M.; Santamaría, A.; Hernández-Bagaces, J.J.; Ortega-López, V. Temporal flowability evolution of slag-based self-compacting concrete with recycled concrete aggregate. *J. Clean. Prod.* **2021**, *299*, 126890. [CrossRef]

23. Pedro, D.; de Brito, J.; Evangelista, L. Evaluation of high-performance concrete with recycled aggregates: Use of densified silica fume as cement replacement. *Constr. Build. Mater.* **2017**, *147*, 803–814. [CrossRef]

24. Akbulut, Z.F.; Yavuz, D.; Tawfik, T.A.; Smarzewski, P.; Guler, S. Examining the Workability, Mechanical, and Thermal Characteristics of Eco-Friendly, Structural Self-Compacting Lightweight Concrete Enhanced with Fly Ash and Silica Fume. *Materials* **2024**, *17*, 3504. [CrossRef] [PubMed]

25. Aruchamy, V.; Subramaniyan, Y.; Viswanathan, R.; Manoharan, A. Improving durability and mechanical features of silica fume and waste glass powder in eco-friendly self-compacting concrete. *Rev. Mater.* **2024**, *29*, e20240072. [CrossRef]

26. Manso-Morato, J.; Hurtado-Alonso, N.; Revilla-Cuesta, V.; Skaf, M.; Ortega-López, V. Fiber-Reinforced concrete and its life cycle assessment: A systematic review. *J. Build. Eng.* **2024**, *94*, 110062. [CrossRef]

27. Sonar, K.; Sathe, S. Exploring fiber reinforcements in concrete and its challenges: A comprehensive review. *Multiscale Multidiscip. Model. Exp. Des.* **2024**, *7*, 3099–3131. [CrossRef]

28. Ahmad, J.; Zhou, Z.; Deifalla, A.F. Steel Fiber Reinforced Self-Compacting Concrete: A Comprehensive Review. *Int. J. Concr. Struct. Mater.* **2023**, *17*, 51. [CrossRef]

29. Thomas, L.; Ramachandra, M. Advanced materials for wind turbine blade—A Review. *Mater. Today Proc.* **2018**, *5*, 2635–2640. [CrossRef]

30. Rani, M.; Choudhary, P.; Krishnan, V.; Zafar, S. A review on recycling and reuse methods for carbon fiber/glass fiber composites waste from wind turbine blades. *Compos. Part B Eng.* **2021**, *215*, 108768. [CrossRef]

31. Joustra, J.; Flipsen, B.; Balkenende, R. Structural reuse of wind turbine blades through segmentation. *Compos. Part C Open Access* **2021**, *5*, 100137. [CrossRef]

32. Liu, P.; Barlow, C.Y. Wind turbine blade waste in 2050. *Waste Manag.* **2017**, *62*, 229–240. [CrossRef] [PubMed]

33. Baturkin, D.; Masmoudi, R.; Tagnit-Hamou, A.; Metiche, S.; Massicotte, L. Feasibility Study on the Recycling of FRP Materials from Wind Turbine Blades in Concrete. *Lect. Notes Civ. Eng.* **2022**, *198*, 1729–1742. [CrossRef]

34. Yazdanbakhsh, A.; Bank, L.C.; Rieder, K.A.; Tian, Y.; Chen, C. Concrete with discrete slender elements from mechanically recycled wind turbine blades. *Resour. Conserv. Recycl.* **2018**, *128*, 11–21. [CrossRef]

35. Wei, Y.; Hadigheh, S.A. Development of an innovative hybrid thermo-chemical recycling method for CFRP waste recovery. *Compos. Part B Eng.* **2023**, *260*, 110786. [CrossRef]

36. Fonte, R.; Xydis, G. Wind turbine blade recycling: An evaluation of the European market potential for recycled composite materials. *J. Environ. Manag.* **2021**, *287*, 112269. [CrossRef]

37. Wei, Y.; Hadigheh, S.A. Enhancing carbon fibre recovery through optimised thermal recycling: Kinetic analysis and operational parameter investigation. *Mater. Today Sustain.* **2024**, *25*, 100661. [CrossRef]

38. Tao, S.; Zhang, C.; Feijóo, A.; Kim, V. Wind farm repowering optimization: A techno-economic-aesthetic approach. *IET. Renew. Power Gener.* **2023**, *17*, 2137–2147. [CrossRef]

39. Xu, G.T.; Liu, M.J.; Xiang, Y.; Fu, B. Valorization of macro fibers recycled from decommissioned turbine blades as discrete reinforcement in concrete. *J. Clean. Prod.* **2022**, *379*, 134550. [CrossRef]

40. Revilla-Cuesta, V.; Skaf, M.; Ortega-López, V.; Manso, J.M. Raw-crushed wind-turbine blade: Waste characterization and suitability for use in concrete production. *Resour. Conserv. Recycl.* **2023**, *198*, 107160. [CrossRef]

41. Revilla-Cuesta, V.; Manso-Morato, J.; Hurtado-Alonso, N.; Skaf, M.; Ortega-López, V. Mechanical and environmental advantages of the revaluation of raw-crushed wind-turbine blades as a concrete component. *J. Build. Eng.* **2024**, *82*, 108383. [CrossRef]

42. Pinto, H.; Nepomuceno, M.; Bernardo, L.; Oliveira, L. Experimental evaluation of the potential use of waste recycled concrete fine aggregates to produce self-compacting concrete. *AIP Conf. Proc.* **2023**, *2928*, 080033. [CrossRef]
43. Roussel, N. *Understanding the Rheology of Concrete*; Elsevier Ltd.: Amsterdam, The Netherlands, 2011; pp. 1–364. [CrossRef]
44. Tavangar, T.; Hosseinpoor, M.; Yahia, A.; Khayat, K.H. Computational investigation of concrete pipe flow: Critical review. *ACI Mater. J.* **2021**, *118*, 203–215. [CrossRef]
45. Thrane, L.; Bras, A.; Bakker, P.; Brameshuber, W.; Cazacliu, B.; Ferrara, L.; Feys, D.; Geiker, M.; Gram, A.; Grünewald, S.; et al. Computational fluid dynamics. *RILEM State Art Rep.* **2014**, *15*, 25–63. [CrossRef]
46. Orbe, A.; Losada, R.; Rojí, E.; Cuadrado, J.; Maturana, A. The prediction of bending strengths in SFRSCC using Computational Fluid Dynamics (CFD). *Constr. Build. Mater.* **2014**, *66*, 587–596. [CrossRef]
47. Kulasegaram, S.; Karihaloo, B.L. Fibre-reinforced, self-compacting concrete flow modelled by smooth particle hydrodynamics. *Proc. Inst. Civ. Eng. Eng. Comput. Mech.* **2013**, *166*, 22–31. [CrossRef]
48. Bi, J.; Zhao, Y.; Guan, J.; Huo, L.; Qiao, H.; Yuan, L. Three-dimensional modeling of the distribution and orientation of steel fibers during the flow of self-compacting concrete. *Struct. Concr.* **2019**, *20*, 1722–1733. [CrossRef]
49. *EN 197-1*; Cement—Part 1: Composition, Specifications and Conformity Criteria for Common Cements. European Committee for Standardization: Brussels, Belgium, 2011.
50. Zhang, X.; Zhang, C.; Bi, M.; Yang, H.; Sun, H.; Mu, R. Optimization of Mix Proportion of Self-compacting Concrete Based on Single Fluid Model. *KSCE J. Civ. Eng.* **2022**, *26*, 1282–1294. [CrossRef]
51. *EN 933-1*; Tests for Geometrical Properties of Aggregates—Part 1: Determination of Particle Size Distribution—Sieving Method. European Committee for Standardization: Brussels, Belgium, 2012.
52. *EN 933-8*; Tests for Geometrical Properties of Aggregates—Part 8: Assessment of Fines—Sand Equivalent Test. European Committee for Standardization: Brussels, Belgium, 2016.
53. *EN 1097-6*; Tests for Mechanical and Physical Properties of Aggregates—Part 6: Determination of Particle Density and Water Absorption. European Committee for Standardization: Brussels, Belgium, 2014.
54. *EN 933-3*; Tests for Geometrical Properties of Aggregates—Part 3: Determination of Particle Shape—Flakiness Index. European Committee for Standardization: Brussels, Belgium, 2012.
55. *EN 1744-1*; Tests for Chemical Properties of Aggregates—Part 1: Chemical Analysis. European Committee for Standardization: Brussels, Belgium, 2013.
56. Islam, M.J.; Shahjalal, M.; Haque, N.M.A. Mechanical and durability properties of concrete with recycled polypropylene waste plastic as a partial replacement of coarse aggregate. *J. Build. Eng.* **2022**, *54*, 104597. [CrossRef]
57. *EN 206*; Concrete—Specification, Performance, Production and Conformity. European Committee for Standardization: Brussels, Belgium, 2021.
58. *EN 12350-8*; Testing Fresh Concrete—Part 8: Self-Compacting Concrete—Slump-Flow Test. European Committee for Standardization: Brussels, Belgium, 2020.
59. *EN 12350-10*; Testing Fresh Concrete—Part 10: Self-Compacting Concrete—L Box Test. European Committee for Standardization: Brussels, Belgium, 2011.
60. *EN 12350-12*; Testing Fresh Concrete—Part 12: Self-Compacting Concrete—J-Ring Test. European Committee for Standardization: Brussels, Belgium, 2011.
61. EFNARC. *Specifications and Guidelines for Self-Compacting Concrete*; EFNARC: Surrey, UK, 2002.
62. Flow3D Software. 2024. Available online: https://www.flow3d.com/products/flow-3d/ (accessed on 22 October 2024).
63. Karakurt, C.; Çelik, A.O.; Yılmazer, C.; Kiriççi, V.; Özyaşar, E. CFD simulations of self-compacting concrete with discrete phase modeling. *Constr. Build. Mater.* **2018**, *186*, 20–30. [CrossRef]
64. Baluch, M.H.; Rahman, M.K.; Mukhtar, F.; Malik, M.A. A 2-D computational fluid dynamics simulation of slump flow and L-box test on SCC using ANSYS/FLUENT. In Proceedings of the Annual Conference—Canadian Society for Civil Engineering, Ottawa, ON, Canada, 14–17 June 2011; Volume 2, pp. 1331–1338.
65. *EN 12390-2*; Testing Hardened Concrete—Part 2: Making and Curing Specimens for Strength Tests. European Committee for Standardization: Brussels, Belgium, 2020.
66. *EN 12390-3*; Testing Hardened Concrete—Part 3: Compressive Strength of Test Specimens. European Committee for Standardization: Brussels, Belgium, 2020.
67. *EN 12390-13*; Testing Hardened Concrete—Part 13: Determination of Secant Modulus of Elasticity in Compression. European Committee for Standardization: Brussels, Belgium, 2022.
68. *EN 12390-6*; Testing Hardened Concrete—Part 6: Tensile Splitting Strength of Test Specimens. European Committee for Standardization: Brussels, Belgium, 2024.
69. *EN 12390-5*; Testing Hardened Concrete—Part 5: Flexural Strength of Test Specimens. European Committee for Standardization: Brussels, Belgium, 2020.
70. Jang, E.S.; Kang, C.W. Porosity analysis of three types of balsa (*Ochroma pyramidale*) wood depending on density. *J. Wood Sci.* **2022**, *68*, 31. [CrossRef]
71. *EN 12350-11*; Testing Fresh Concrete—Part 11: Self-Compacting Concrete—Sieve Segregation Test. European Committee for Standardization: Brussels, Belgium, 2010.

72. Bentegri, I.; Boukendakdji, O.; Kadri, E.H.; Ngo, T.T.; Soualhi, H. Rheological and tribological behaviors of polypropylene fiber reinforced concrete. *Constr. Build. Mater.* **2020**, *261*, 119962. [CrossRef]

73. Revilla-Cuesta, V.; Skaf, M.; Ortega-López, V.; Manso, J.M. Multi-parametric flowability classification of self-compacting concrete containing sustainable raw materials: An approach to real applications. *J. Build. Eng.* **2023**, *63*, 105524. [CrossRef]

74. Cantero, B.; Bravo, M.; de Brito, J.; Sáez del Bosque, I.F.; Medina, C. Mechanical behaviour of structural concrete with ground recycled concrete cement and mixed recycled aggregate. *J. Clean. Prod.* **2020**, *275*, 122913. [CrossRef]

75. Revilla-Cuesta, V.; Serrano-López, R.; Espinosa, A.B.; Ortega-López, V.; Skaf, M. Analyzing the Relationship between Compressive Strength and Modulus of Elasticity in Concrete with Ladle Furnace Slag. *Buildings* **2023**, *13*, 3100. [CrossRef]

76. Trento, D.; Faleschini, F.; Revilla-Cuesta, V.; Ortega-López, V. Improving the early-age behavior of concrete containing coarse recycled aggregate with raw-crushed wind-turbine blade. *J. Build. Eng.* **2024**, *92*, 109815. [CrossRef]

77. *CEN EN 1992-1-1:2010*; EC-2 Eurocode 2: Design of Concrete Structures. Part 1-1: General Rules and Rules for Buildings. CEN European Committee for Standardization: Brussels, Belgium, 2010.

78. Ouchi, M.; Hibino, M.; Okamura, H. Effect of superplasticizer on self-compactability of fresh concrete. *Transp. Res. Rec.* **1996**, *1574*, 37–40. [CrossRef]